

# **Low Energy Electron Diffraction**

## **Group C**

Zhan Yi Bill Chng, zchng@smail.uni-koeln.de  
Alexander Bott, s6albott@uni-bonn.de

Supervisor: Morris Mühlpointner

Days in the laboratory: 27.06.2024

First submission: 04.07.2024

Second submission: 14.07.2024

In this experiment, an Au(111) surface was studied with low energy electron diffraction (LEED). From the LEED-pattern of the Au(111) sample, the distance of the sample to the LEED-screen, the surface lattice constant, as well as the bulk lattice constant can be deduced. LEED was also used to study the reconstruction of the Au(111) surface in vacuum, and the formation of blue phosphorus following the adsorption of phosphorus.

## Contents

<b>1</b>	<b>Introduction</b>	<b>2</b>
1.1	Electron beam diffraction . . . . .	2
1.2	LEED and the reciprocal lattice . . . . .	3
1.2.1	The Ewald construction . . . . .	3
1.2.2	The reciprocal lattice . . . . .	4
1.3	The Au(111) surface and its applications . . . . .	4
<b>2</b>	<b>Methodology</b>	<b>6</b>
2.1	Experimental setup . . . . .	6
2.2	Experimental procedure . . . . .	7
2.2.1	Sample cleaning . . . . .	7
2.2.2	LEED Experiments . . . . .	7
2.3	Blue Phosphorus Experiment Attempt . . . . .	7
<b>3</b>	<b>Results</b>	<b>8</b>
3.1	Orientation of the surface . . . . .	8
3.2	Determination of the spot distances . . . . .	9
3.3	Determination of the Au(111) surface lattice constant . . . . .	13
3.4	Au(111) reconstruction analysis . . . . .	16
3.5	LEED pattern for Blue Phosphorus on Au (111) . . . . .	17
<b>4</b>	<b>Discussion</b>	<b>18</b>
4.1	Determination of the LEED-screen to sample distance and the lattice constants .	18
4.2	The Au (111) surface reconstruction . . . . .	18
4.3	The P/Au(111) system . . . . .	19
	<b>References</b>	<b>20</b>

# 1 Introduction

## 1.1 Electron beam diffraction

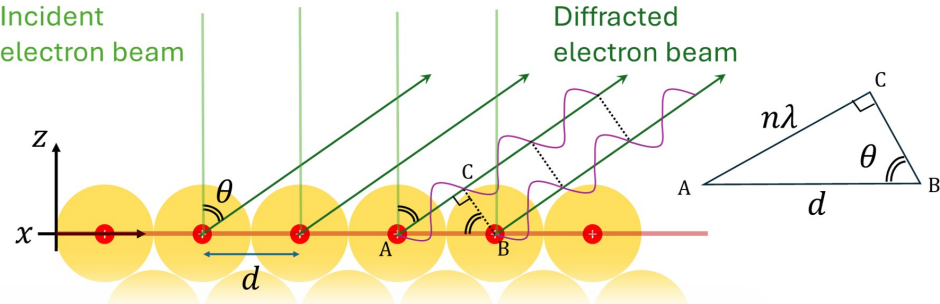


Figure 1: A model illustrating the derivation of the diffraction grating equation for LEED.

Low Energy Electron Diffraction (LEED) is a surface sensitive diffraction technique used to study the lattice structure of crystalline solids. An electron beam is directed onto the surface of a crystalline sample and diffracted, which transforms a regularly repeating surface lattice in real space into a reciprocal lattice in  $k$ -space. More specifically, LEED takes a series of Miller lines ( $hk$ ) on the surface of the lattice and maps it onto a diffraction spot. The surface sensitivity of electron diffraction arises from the much shorter penetration depth of a low energy electron beam, as it interacts with the surface atoms inelastically and loses kinetic energy. In general, the penetration depth of an electron beam is governed by its inelastic mean free path,  $\Lambda$ , which is dependent on its kinetic energy,  $E_k$ .<sup>[1]</sup>

$$\Lambda(E_k) = \frac{1430}{E_k^2} + 0.54\sqrt{E_k} \quad (1)$$

where  $\Lambda(E_k)$  is in units of Å, and  $E$  is given in eV.

Using Equation (1), one could show that a low energy electron beam with an  $E_k$  of 10 to 200 eV would have a  $\Lambda$  of 8 to 16 Å, corresponding to several atomic layers into the bulk crystal. This consequently limits electron diffraction to just a surface phenomenon. Assuming electron diffraction is primarily caused by surface atoms, LEED can be described by the diffraction grating equation (see Figure 1), as follows:

$$n\lambda_e = d \sin(\theta) \quad (2)$$

where  $\lambda_e$  is the electron wavelength,  $d$  is the spacing between lattice points in real space, and  $\theta$  is the diffraction angle.  $n$  determines the order of the diffraction spot, and can take values of 1, 2, 3... . To find  $\lambda_e$ , one must treat the electron like a wave and use the de Broglie relationship:

$$\lambda_e = \frac{h}{p}. \quad (3)$$

$h$  is Planck's constant and  $p$  is the momentum of the electron. Since the kinetic energy of the electron  $E_k = \frac{p^2}{2m_e}$ , the de Broglie equation can be expressed in terms of  $E_k$ :

$$\lambda_e = \sqrt{\frac{h^2}{2m_e E_k}}. \quad (4)$$

$\frac{h^2}{2m_e}$  is a constant with dimensions of energy. Hence, this can be expressed as a single energy value in units of eV, which allows for  $E_k$  to be in eV as well:

$$\lambda_e = \sqrt{\frac{150.4 \text{ eV}}{E_k}} \cdot [\text{\AA}]. \quad (5)$$

This conveniently outputs  $\lambda_e$  in units of Å.

## 1.2 LEED and the reciprocal lattice

### 1.2.1 The Ewald construction

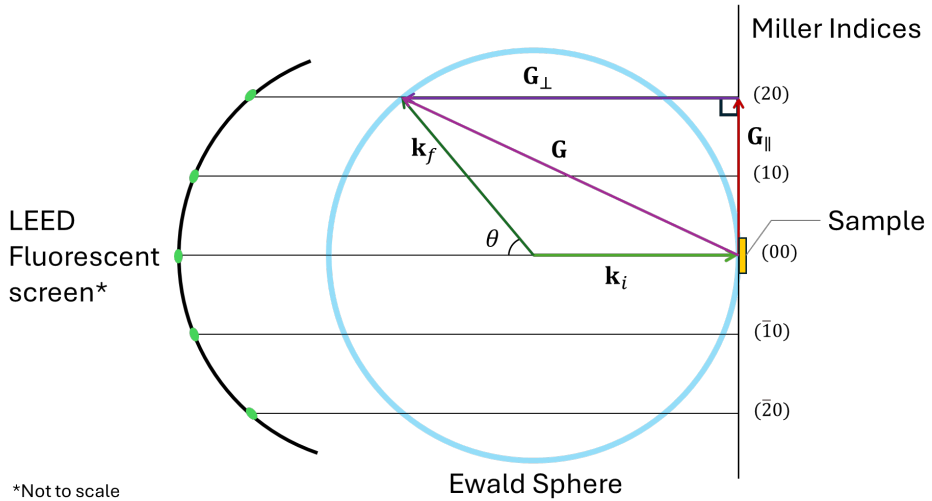


Figure 2: Cross section of an Ewald Sphere, indicating how Miller lines ( $hk$ ), i.e., lattice points with the same  $\mathbf{G}_{\parallel}$ , map onto the same point on the LEED pattern.  $\mathbf{k}_i$  is the incident electron wavevector,  $\mathbf{k}_f$  is the elastically diffracted electron wavevector,  $\mathbf{G}$  is the reciprocal lattice vector, and  $\mathbf{G}_{\perp}$ ,  $\mathbf{G}_{\parallel}$  are the perpendicular and parallel components of  $\mathbf{G}$  respectively.

As mentioned, LEED transforms a surface lattice in real space into its reciprocal lattice. This can be understood *via* the Ewald construction (Figure 2), which uses the Ewald sphere, a sphere whose radius is the magnitude of the electron beam wavevector,  $k_0$ . Referring to Figure 2, the following relations hold:<sup>[2]</sup>

$$k_0 = k_i = k_f = \frac{2\pi}{\lambda_e} \quad (6)$$

$$\mathbf{G} = \mathbf{k}_f - \mathbf{k}_i \quad (7)$$

$$\mathbf{G} = \mathbf{G}_{\parallel} + \mathbf{G}_{\perp} = h\mathbf{a}_1^* + k\mathbf{a}_2^* + \mathbf{G}_{\perp}, \quad (8)$$

where  $\mathbf{a}_1^*$  and  $\mathbf{a}_2^*$  are the reciprocal surface unit cell basis vectors. In the case for Figure 2, the

cross section of the Ewald sphere is aligned with  $\mathbf{a}_2^*$ . Since  $|\mathbf{G}_{\parallel}| = h|\mathbf{a}_1^*| = \mathbf{k}_f \sin \theta$ , this recovers the diffraction grating equation (Equation 1). Thus this model demonstrates the link between diffraction and the process of generating a reciprocal lattice from a surface lattice in real space.

### 1.2.2 The reciprocal lattice

Given a surface unit cell with bases  $\mathbf{a}_1$  and  $\mathbf{a}_2$ , the reciprocal basis vectors are given by the following relationship:<sup>[2]</sup>

$$\mathbf{a}_m \cdot \mathbf{a}_n^* = 2\pi \delta_{mn} . \quad (9)$$

In two dimensions  $m, n = 1, 2$ . One could then derive two relationships of practical importance:

$$|\mathbf{a}_1^*| = \frac{2\pi}{|\mathbf{a}_1| \cos(\alpha_1)} \quad (10)$$

$$\mathbf{a}_2^* \perp \mathbf{a}_1 , \quad (11)$$

where  $\alpha_1$  is the angle between  $\mathbf{a}_1$  to  $\mathbf{a}_1^*$ . By symmetry, the same would be true for  $\mathbf{a}_2$ .

### 1.3 The Au(111) surface and its applications

In this study, the Au(111) surface was chosen as the surface of interest. The Au(111) surface is a stable, close-packed surface that is relatively easily prepared, which lends itself to plenty of adsorption studies. One of the few applications of the Au(111) surface is in the synthesis of phosphorene, better known as blue phosphorus, which is a two-dimensional covalent network of phosphorus with a honeycomb lattice. Blue phosphorus is of particular interest amongst semiconductors, as it boasts a band gap that can be tuned by varying the number of layers, or by applying strain.<sup>[3]</sup> The adsorption of phosphorus on an Au(111) surface template facilitates the fabrication of blue phosphorus, hence this topic was a point of interest in this experiment as well.

Applying equations (10) and (11), the reciprocal unit cell of the Au(111) can be predicted, as illustrated in Figure 3. In doing so, however, it is important to take into consideration surface reconstructions. In the case for Au(111), the surface undergoes a  $p(22 \times \sqrt{3})$  "Herringbone" reconstruction, which can be directly observed with Scanning Tunneling Microscopy (STM).<sup>[4]</sup> While LEED is not the definitive characterisation technique for such a large unit cell, the diffraction spots corresponding to the Herringbone reconstruction would still appear on a LEED pattern, albeit very faintly. These reconstruction spots were reportedly observed in diffraction patterns generated *via* Helium Atom Scattering, which uses Helium atoms instead of electrons for diffraction and offers better surface sensitivity.<sup>[5]</sup>

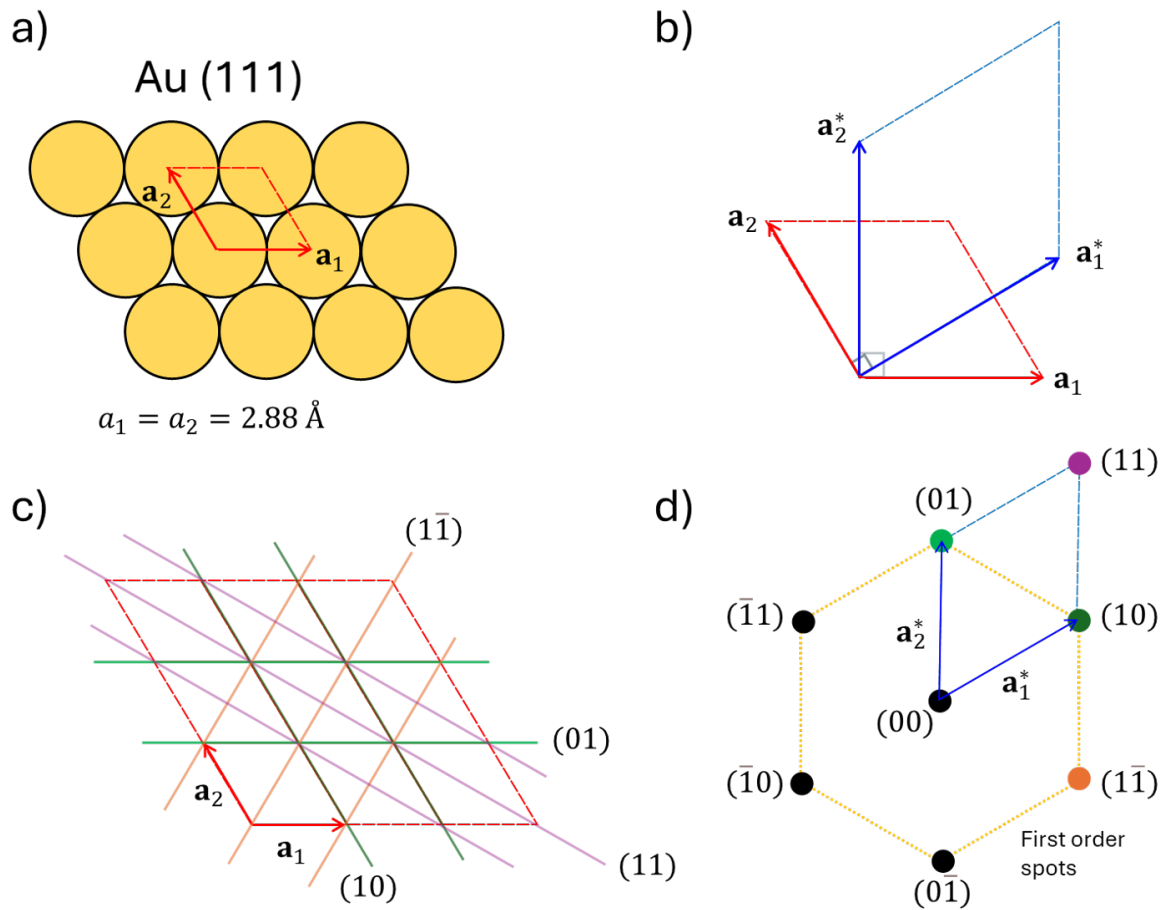


Figure 3: a) The surface unit cell of an unreconstructed Au(111) surface. b) A visualisation of the reciprocal surface unit cell, following the rules stated in (Equations (10) and (11)). c) Miller lines for the Au(111) unit cell. d) The resulting LEED pattern for unreconstructed Au(111).

## 2 Methodology

### 2.1 Experimental setup

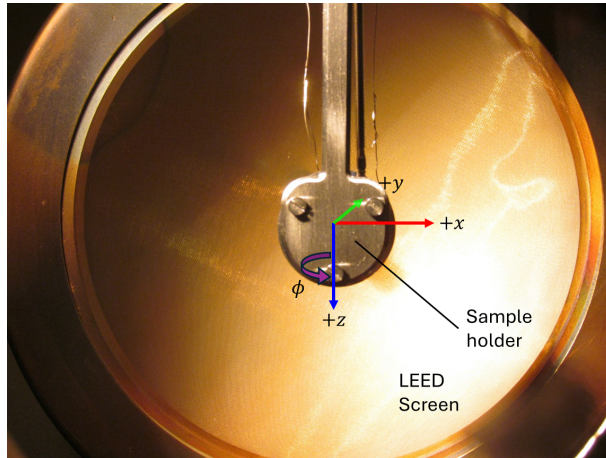


Figure 4: A photo of the LEED screen along with the sample holder, annotated with the degrees of freedom the sample can be moved in the vacuum chamber.

The LEED experiment was conducted in a chamber kept under ultra high vacuum (UHV) conditions, *i.e.*,  $ca.$   $10^{-10}$  mbar, with a turbomolecular pump. In this experiment, however, the chamber pressure was higher than ideal ( $p = 3.4 \cdot 10^{-9}$  mbar). The sample used was an Au(111) surface, which was mounted on a sample holder connected to a manipulator. The sample can be rotated along the z-axis through an angle,  $\phi$ , as well as translated along the x, y, and z axes - these four degrees of freedom make up the coordinates of the sample ( $x, y, z, \phi$ ) (Figure 4). *Nota bene*,  $x$ ,  $y$ , and  $z$  are in units of mm.

Using a Wehnelt electron gun, electrons are accelerated onto the surface of the sample and diffracted. The filament of the Wehnelt gun, where free electrons are generated *via* thermionic emission, is set at a voltage,  $V_f$ , whereas the sample is grounded. Since  $V_f$  is a negative number,  $\Delta V = -V_f$ , which also gives the energy of the electron beam in eV. This can then be used to determine the wavelength of the diffracted electron using Equation (5). To deflect and focus the electron beam, a series of positive electrodes  $Y_1$ ,  $Y_2$ ,  $X_2$ , and  $X_3$  are used. A bias voltage is also applied on the Wehnelt cylinder to focus the electron stream. These voltages, along with  $V_f$ , are collectively known as lens voltages, which were manipulated in the LEED experiment to produce a high quality diffraction pattern.

After the incident electron beam hits the sample, it is diffracted onto the fluorescent screen – the brighter the fluorescence, the higher the intensity of the diffracted spot. However, not all electrons that encounter the fluorescent screen are of the same energy, as some electrons lose energy as they interact with the sample surface inelastically, resulting in a change in both kinetic energy and direction. This phenomenon results in the blurring of diffraction spots on the fluorescent screen. To counteract this problem, suppressor screens, which are negatively charged mesh screens placed in front of the fluorescent screen, are used to filter out inelastic electrons. The voltage applied on the suppressor screens can thus be fine tuned to produce a high contrast, sharp diffraction pattern.

## 2.2 Experimental procedure

### 2.2.1 Sample cleaning

The cleaning procedure was carried out the day before by the supervisor, Morris Mühlpointner. Impurities on the Au(111) surface were cleaned by sputtering Ar<sup>+</sup> ions. The energy of the Ar<sup>+</sup> beam was set at 1 keV, and Argon was dosed at a pressure of  $1 \cdot 10^{-5}$  mbar. The sample surface was then annealed up to a temperature of 973 K for 90 minutes, and then left to cool down.

### 2.2.2 LEED Experiments

For each LEED pattern generated, a photo was taken with a Canon PowerShot SX30 IS digital camera. The photos were then subsequently analysed.

In the first experiment, the dependence of the LEED pattern on the incident angle of the electron beam was studied. The sample was first placed at a coordinate of (22.0, 15.0, 0.0, 280°). The beam energy was fixed at 125.5 eV. The camera settings were as follows: ISO = 400, Aperture = f/4.5, Exposure = 10 s, Zoom = 30 cm. The resultant LEED pattern at  $\phi = 280^\circ$  was recorded. This was repeated for displacements in  $\phi$ , labelled  $\theta$ , of 5°, 10°, 15°, and 20° in both directions, *i.e.*,  $260^\circ \leq \phi \leq 300^\circ$  in 5° intervals.

The dependence of the LEED pattern on beam energy was also studied. This time,  $\phi$  was fixed at 279.5° and the camera settings remain unchanged. Four distinct LEED patterns were generated and recorded at four different energies: 100.0 eV, 130.1 eV, 160.1 eV, and 200 eV.

To observe the Au(111) reconstruction, the sample was intentionally rotated to  $\phi = 282.3^\circ$  to uncover the (0,0) spot. The beam energy was optimised at 97.7 eV to ensure that the satellite spots are their most visible. A photo of this LEED pattern was once again taken with the same camera settings.

## 2.3 Blue Phosphorus Experiment Attempt

To deposit phosphorus onto the Au(111) sample surface, the sample was first positioned in front of the phosphorus evaporator. The sample was therefore moved to a new coordinate of (11.15, 24.0, 48.425, 43.4°) using the manipulator. Phosphorus was dosed at a cell temperature of 254 °C (527.15 K) and a pressure of  $4.0 \cdot 10^{-8}$  mbar. The surface was then moved back to (22.0, 15.0, 0, 279.5°) for LEED, at an energy of 150 eV. Unfortunately, upon inspection, no blue phosphorus spots were observed. A photo of a LEED pattern of blue phosphorus prepared previously by Mühlpointner and others was therefore used in further analyses. The preparation was similar – phosphorus was evaporated onto Au(111) at 550 K for 45 minutes, and then a Spot Profile Analysis LEED (SPA-LEED) pattern was generated at 68 eV.

### 3 Results

All LEED photos were analysed using Spot-Plotter, and further analyses with the resulting data were carried out on Origin.

#### 3.1 Orientation of the surface

The surface at hand is an Au(111) surface, so an fcc unit cell building an hexagonal surface. The picture, which is seen in Figure 5, was taken at an energy of 160.1 eV, so not only the first order spots, but also the second and third order spots are visible. With this, the surface unit cell of the reciprocal realm could be marked, created out of the reciprocal lattice vectors  $\mathbf{a}^*$  and  $\mathbf{b}^*$ . For comparison a *fcc*(111) surface with the surface unit cell in real space is sketched below. Here the unit cell is created out of the lattice vectors  $\mathbf{a}$  and  $\mathbf{b}$ , with  $\mathbf{a}$  perpendicular to  $\mathbf{b}^*$  and  $\mathbf{b}$  perpendicular to  $\mathbf{a}^*$ .

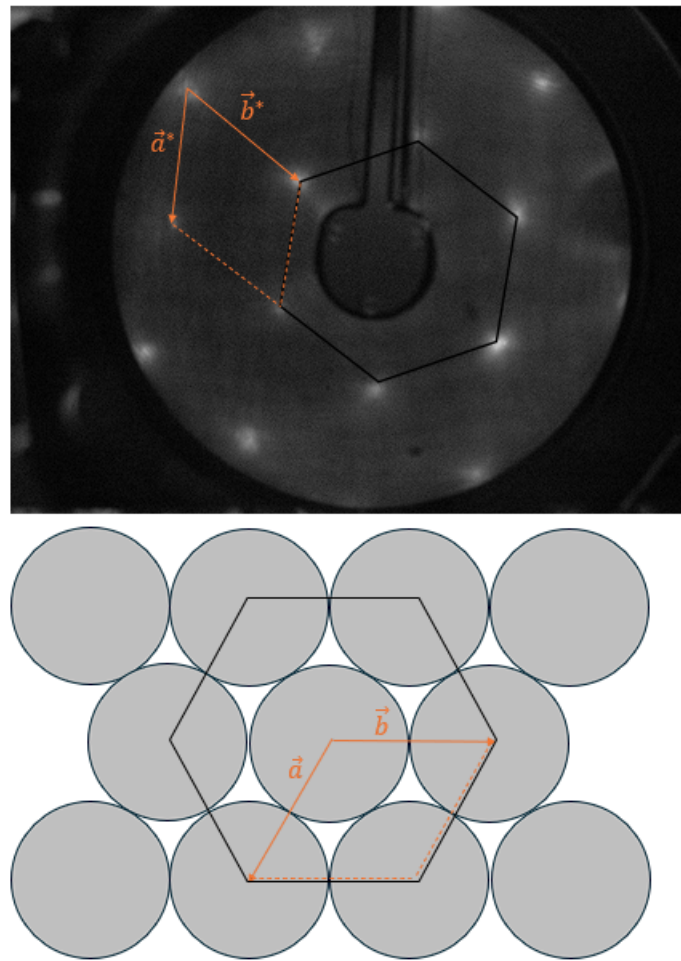


Figure 5: In the picture at the top is a LEED pattern of an Au(111) surface at an energy of 160.1 eV, below is a hard-sphere-model of a fcc(111) surface. In black marked is the hexagonal structure, in orange marked are the lattice vectors of the primitive unit cell in the reciprocal space in the LEED pattern,  $\mathbf{a}^*$  and  $\mathbf{b}^*$ , and in the real space in the hard-sphere-model,  $\mathbf{a}$  and  $\mathbf{b}$ . The resolution of the picture is (1260x945) pixels.

### 3.2 Determination of the spot distances

For the following calculations, the distance  $r$  between the LEED-screen and the sample, or equivalent the screen radius, needs to be determined. To get this quantity, pictures were taken of the LEED pattern while the sample is rotated in respect to its initial rotation. This pictures are seen in Figure 6 and Figure 7.

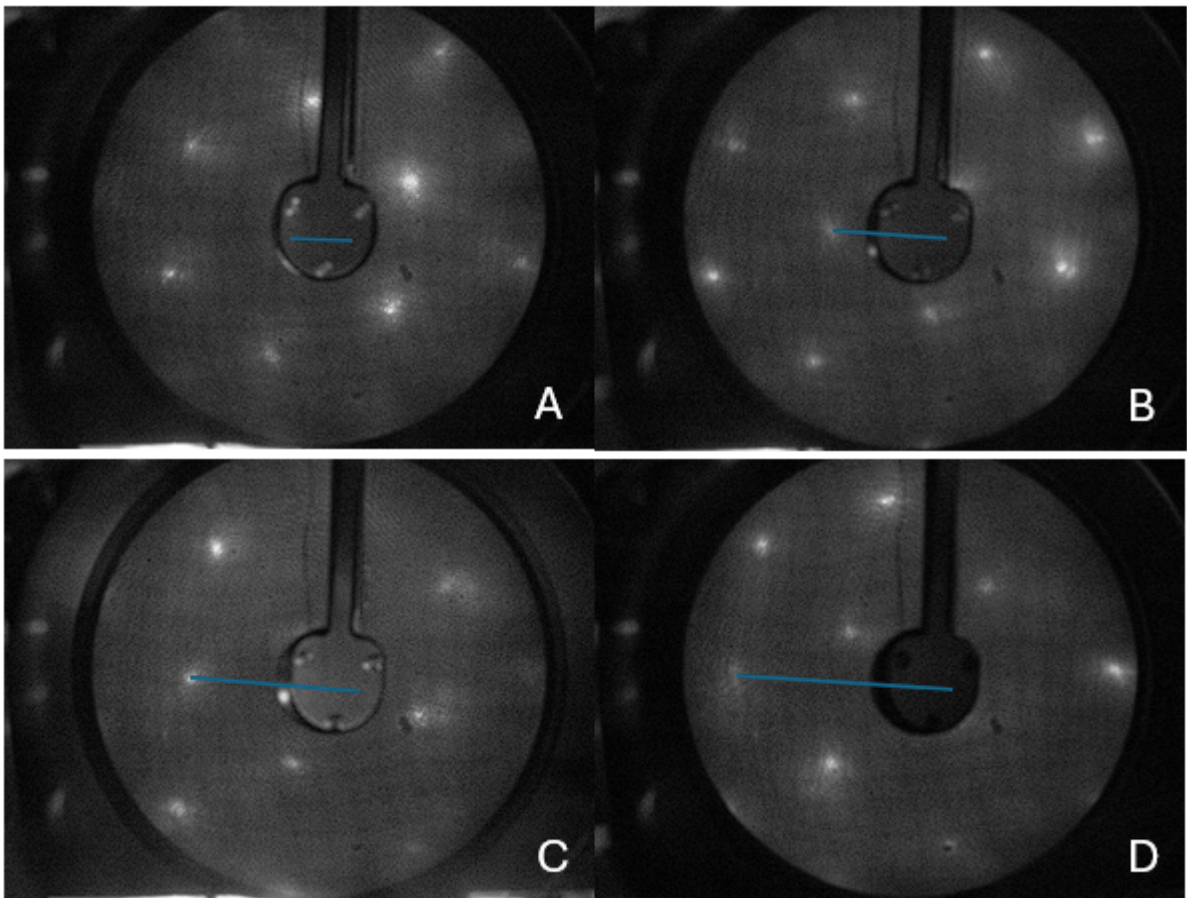


Figure 6: Pictures out of the LEED pattern of the Au(111) surface at four different rotations of the sample in respect to the starting point ( $\theta_A = -5^\circ$ ,  $\theta_B = -10^\circ$ ,  $\theta_C = -15^\circ$ , and  $\theta_D = -20^\circ$ ). In blue sketched is the length of the spot difference of the rotated (0,0)-spot to the initial (0,0)-spot. The resolution of the pictures is (1260x945) pixels.

Visible in this pictures is a shift of the spots seen in the LEED pattern to the left (Figure 6) or to the right (Figure 7). In all the pictures the (0,0)-spot were located and its position was measured. This data can be found in Table 1.

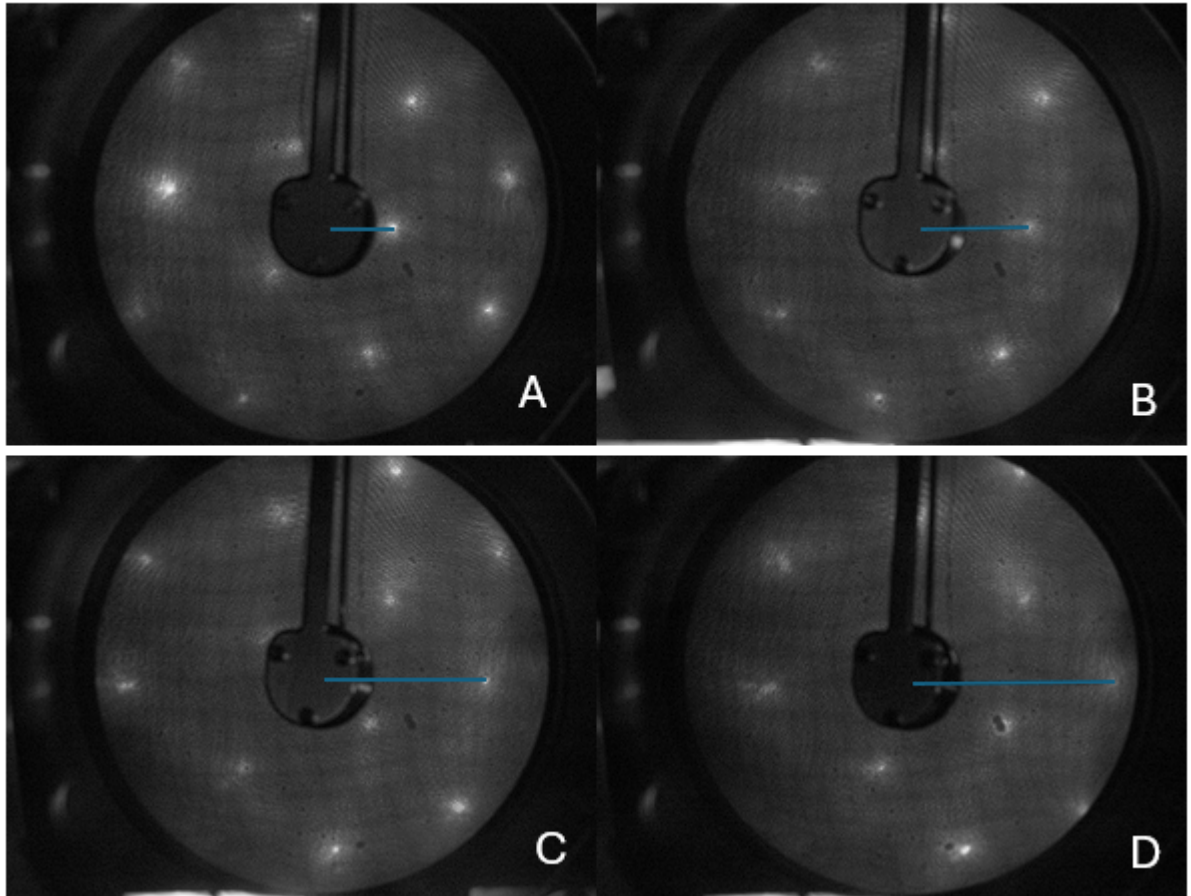


Figure 7: Pictures out of the LEED pattern of the Au(111) surface at four different rotations of the sample in respect to the starting point ( $\theta_A = 5^\circ$ ,  $\theta_B = 10^\circ$ ,  $\theta_C = 15^\circ$ , and  $\theta_D = 20^\circ$ ). In blue sketched is the length of the spot difference of the rotated (0,0)-spot to the initial (0,0)-spot. The resolution of the pictures is (1260x945) pixels.

Table 1: Measured positions  $x$  in pixels of the (0,0)-spot, first before rotation, then with eight different rotations. The distance  $\Delta x$  in pixels between the initial spot and the rotated spots was calculated.

$\theta [^\circ]$	$x$ [pixel]	$\Delta x$ [pixel]
0	700	0
-5	605	95
-10	503	197
-15	398	302
-20	299	401
+5	825	125
+10	925	225
+15	1025	325
+20	1104	404

With the distance  $\Delta x$  and the rotation  $\theta$ , the LEED-screen to sample distance  $r$  can be calculated. It is necessary to be careful about the angle  $\theta$ , which is used here. This angle only describes

the rotation in respect to the initial position of the sample. If an electron beam is now directed towards the surface, it will hit the surface with the angle  $\theta$  and will leave the surface with the same angle  $\theta$ , resulting in a reflection angle of  $2\theta$  to the LEED pattern.

This gives the following equation:

$$\sin(2 \cdot |\theta|) = \frac{\Delta x}{r}. \quad (12)$$

Using this equation,  $\sin(2 \cdot |\theta|)$  is plotted against the (0,0)-spot differences  $\Delta x$  for both rotation-directions in Figure 8.

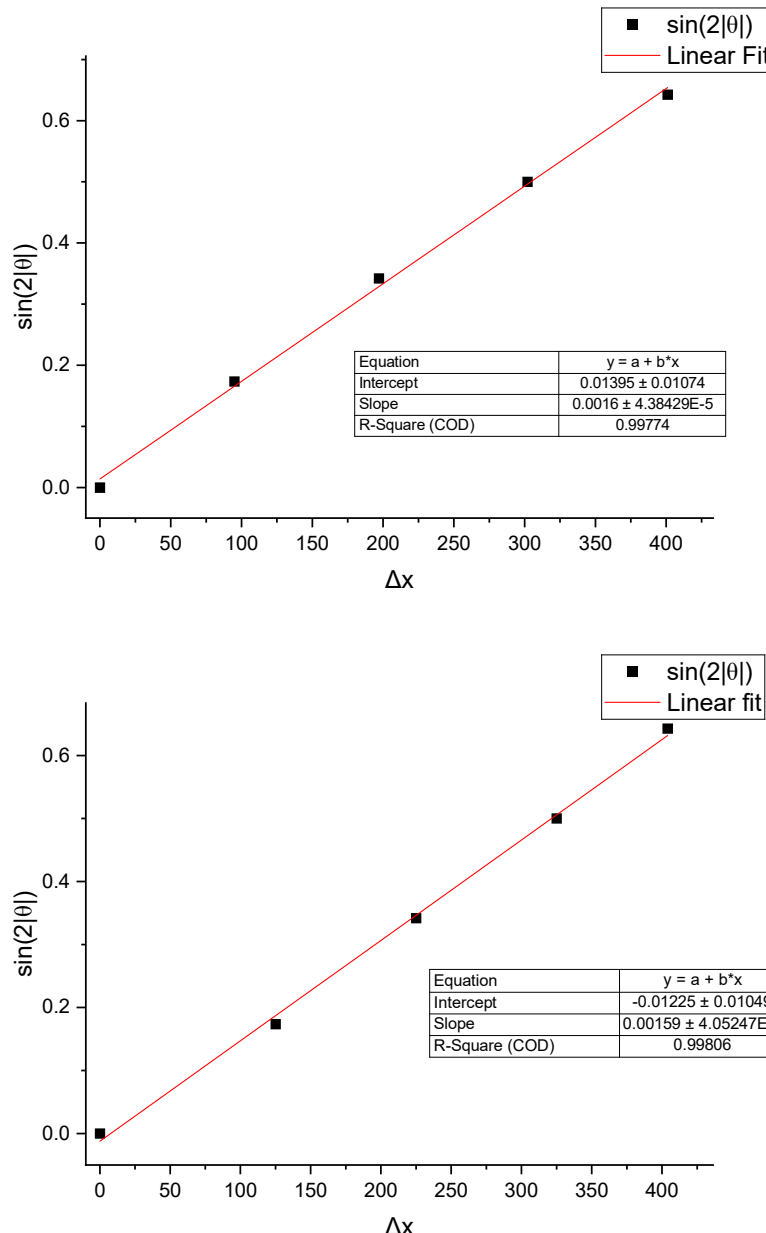


Figure 8: Plotted data of  $\sin(2 \cdot |\theta|)$  against the (0,0)-spot difference  $\Delta x$ , at the top for the rotations of  $\theta^- = -5^\circ, -10^\circ, -15^\circ$ , and  $-20^\circ$ , at the bottom for the rotations of  $\theta^+ = 5^\circ, 10^\circ, 15^\circ$ , and  $20^\circ$  in respect to the initial rotation angle  $\theta_0$ . In red marked and calculated are the linear fits for both diagrams. For the rotation-direction of  $\theta^-$  the linear fit is given as  $y = 0.0016x + 0.01395$ , for the rotation-direction of  $\theta^+$  its  $y = 0.00159x - 0.01225$ .

Out of the slope of a linear fit of this data  $\frac{1}{r}$  is obtained. This linear fit is only reasonable, if the assumption, that the sample is accurately placed in the middle of the LEED-screen, holds. Looking at both values for  $R^2$  given in the box below both fits, which describes the closeness of the measured points to the fit differing between 0 and 1, shows that the estimation for the linear fit runs near to accurate through the measured points. This leads to the conclusion, that the sample was almost exactly placed in the center of the LEED-screen.

For the two rotation-directions a small difference in  $r$  has been measured, with  $r^- = 625 \pm 17.1$  pixels and  $r^+ = 629 \pm 16.0$  pixels. The average of this two gives the guess for  $r$  as  $r = 627 \pm 16.6$  pixels.

### 3.3 Determination of the Au(111) surface lattice constant

In the following the surface lattice constant for the Au(111) surface and the bulk lattice constant for gold were determined. For this, pictures of the LEED pattern at four different energies were taken, which are seen below in Figure 9.

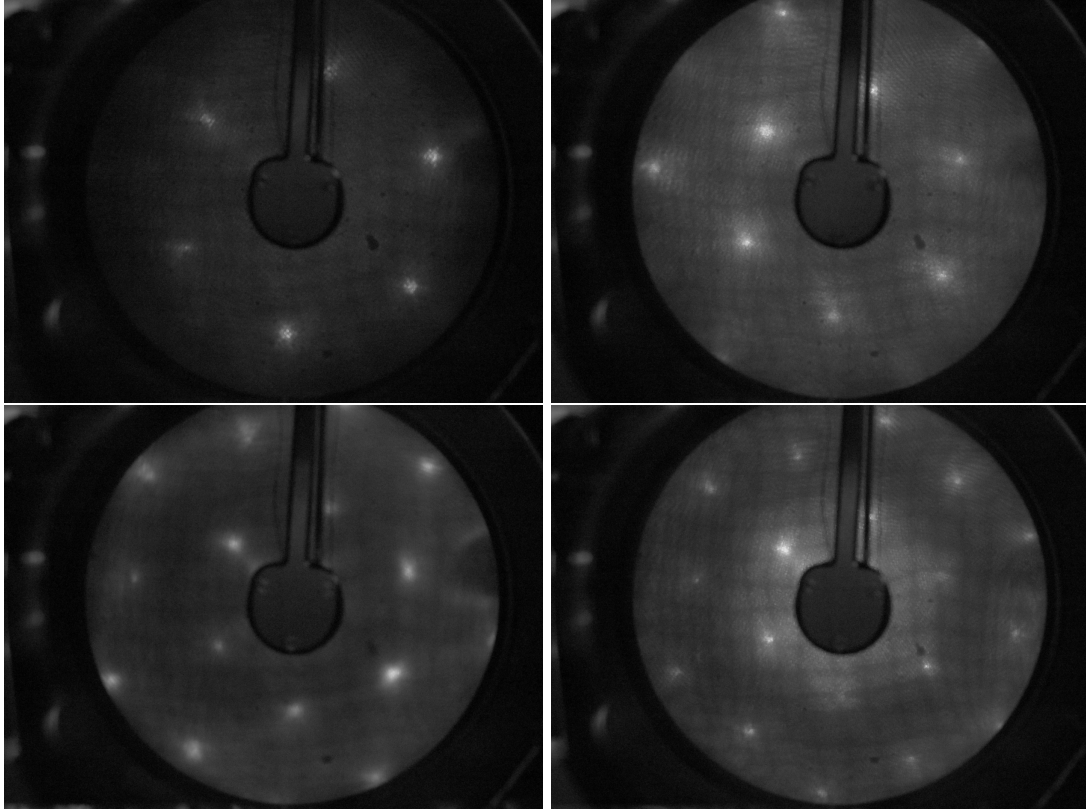


Figure 9: Pictures of the LEED pattern of the Au(111) surface at four different energies (top-left 100.0 eV, top-right 130.1 eV, bottom-left 160.1 eV, and 200.0 eV). All pictures are at a resolution of (1260x945) pixels.

Taking the different energies, the four different electron wavelengths  $\lambda_e$  can be calculated with Equation (5). Using this electron wavelength in Equation (6),  $|\mathbf{k}_0|$  can be calculated. Now needed is the distance between the (0,0)-spot and the surrounding first order spots at the four different energies, which are measured in the pictures in Figure 9. With the in task 3.2 calculated LEED-screen to sample distance  $r$ , the reciprocal surface lattice vector  $|\mathbf{a}^*|$  can be calculated with Equation (13):

$$a^* = |\mathbf{a}^*| = \frac{d}{r} \cdot |\mathbf{k}_0| \quad (13)$$

As we assume an ideal fcc(111) surface in this calculations, the two reciprocal lattice vectors  $|\mathbf{a}^*|$  and  $|\mathbf{b}^*|$  have the same length, so it is only needed to calculate one of them and the direction of the measured distance does not matter. Using the calculated  $|\mathbf{a}^*|$  in Equation (14) gives the quantity for the surface lattice vector, also called surface lattice constant,  $a$ , which then can be used to calculate the bulk lattice constant  $a_b$ :

$$a = |\mathbf{a}| = \frac{4\pi}{\sqrt{3} \cdot |\mathbf{a}^*|} \quad (14)$$

$$a_b = |\mathbf{a}_b| = \sqrt{2} \cdot |\mathbf{a}| \quad (15)$$

All this mentioned calculated data can be seen in Table 2.

Table 2: Measured spot differences,  $d$ , in pixels of each of the six first order spots for each of the four energies,  $E$ . In the seventh, separated row is always the average calculated out of the averaged distance,  $\bar{d}$ . Additionally the, with the energies calculated, electron wavelengths  $\lambda_e$  and  $k_0$  are listed. With this the magnitudes of the reciprocal lattice vectors,  $a^*$ , the surface lattice vectors,  $a$ , and the bulk lattice constant,  $a_b$ , were calculated for the different and the averaged  $d$ . Additionally error propagation was carried out for all the averaged data following Equation (16).

$E$ [eV]	$\lambda_e$ [\AA]	$k_0$ [\AA $^{-1}$ ]	$d$ [pixel]	$a^*$ [\AA $^{-1}$ ]	$a$ [\AA]	$a_b$ [\AA]
100.0	1.226	5.123	311.7	2.547	2.848	4.028
			314.9	2.573	2.820	3.988
			313.1	2.559	2.836	4.010
			307.8	2.515	2.885	4.080
			300.5	2.456	2.955	4.179
			313.0	2.557	2.837	4.012
			$310.2 \pm 1.0$	$2.534 \pm 0.075$	$2.863 \pm 0.085$	$4.048 \pm 0.120$
130.1	1.075	5.844	273.6	2.550	2.846	4.024
			271.3	2.529	2.869	4.058
			266.7	2.485	2.919	4.128
			265.0	2.470	2.937	4.154
			263.0	2.451	2.960	4.186
			266.9	2.487	2.917	4.125
			$267.7 \pm 1.0$	$2.495 \pm 0.075$	$2.907 \pm 0.087$	$4.112 \pm 0.123$
160.1	0.969	6.483	243.0	2.512	2.888	4.084
			246.9	2.553	2.842	4.019
			243.1	2.513	2.887	4.083
			236.6	2.446	2.966	4.195
			237.4	2.454	2.956	4.180
			236.0	2.440	2.918	4.205
			$240.5 \pm 1.0$	$2.487 \pm 0.076$	$2.918 \pm 0.089$	$4.126 \pm 0.126$
200.0	0.867	7.246	220.0	2.542	2.854	4.037
			223.7	2.584	2.807	3.970
			224.5	2.594	2.796	3.959
			217.3	2.512	2.889	4.085
			216.6	2.503	2.898	4.098
			213.6	2.468	2.939	4.157
			$219.3 \pm 1.0$	$2.534 \pm 0.079$	$2.863 \pm 0.089$	$4.049 \pm 0.126$

Most relevant are the averaged surface lattice constant,  $\bar{a}$ , and the averaged bulk lattice constant,  $\bar{a}_b$ , because an error in measuring the distances  $d$  cannot be exterminated. Additionally error propagation for the averaged calculated data was carried out as follows:

$$\Delta y = \left| \frac{dy}{dx_1} \cdot \Delta x_1 \right| + \left| \frac{dy}{dx_2} \cdot \Delta x_2 \right| + \left| \frac{dy}{dx_3} \cdot \Delta x_3 \right| + \dots , \quad (16)$$

starting with  $\Delta d = \pm 1.0$  pixel and  $\Delta r = \pm 16.6$  pixels.

Noticeable is that the quantities for  $\bar{a}$  and  $\bar{a}_b$  for the energies  $E_1 = 100.0$  eV and  $E_4 = 200.0$  eV are almost equal to each other, for the energies  $E_2 = 130.1$  eV and  $E_3 = 160.1$  eV they are a little bit higher. Even so the surface lattice constant and the bulk lattice constant of  $E_1$  and  $E_4$  are a little bit smaller and the ones of  $E_2$  and  $E_3$  are a little bit higher than the surface lattice constant  $a = 2.8810$  Å (*lit.*) and the bulk lattice constant  $a_b = 4.0743$  Å (*lit.*) found by B. N. Dutta and B. Dayal.<sup>[6]</sup>, the total averages of  $\bar{a}$  and  $\bar{a}_b$  would be  $a_{\text{total}} = 2.888 \pm 0.088$  Å and  $a_{b,\text{total}} = 4.084 \pm 0.124$  Å. These quantities are reasonably close to that found in the literature<sup>[6]</sup> to the point that both values are within the range of the calculated errors of the experimental data.

### 3.4 Au(111) reconstruction analysis

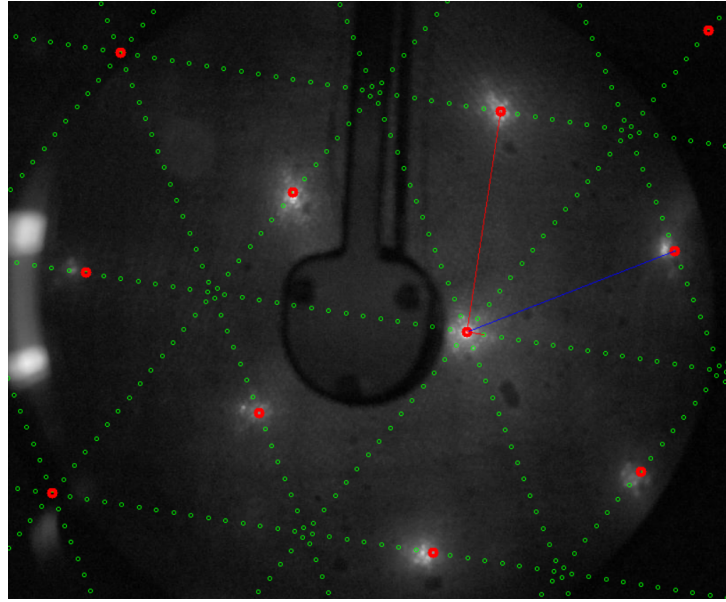


Figure 10: LEED pattern of the Au(111) surface containing reconstruction spots. The (111) underlayer spots are labelled red, whereas the reconstruction spots are highlighted green. The reciprocal surface unit cell of the (111) underlayer as well as the reconstructed overlayer are shown, with blue and red reciprocal unit cell basis vectors respectively.

To observe the reconstruction pattern, the (0,0)-spot as well as the first order spots must be within view. This corresponded to the 100.0 eV LEED pattern as shown in Figure 9. Thus, a beam energy of 97.7 eV was chosen after fine tuning, which produced the sharpest reconstruction spots. The resulting LEED pattern (Figure 10) showed diffraction spots corresponding a reconstructed supercell. Using the reconstruction spots closest to (0,0), an overlayer matrix,  $\mathbf{M}$ , was fitted, which describes the reconstructed overlayer in terms of the unreconstructed Au(111) surface unit cell:

$$\mathbf{M} = \begin{pmatrix} 11.00 & 0.00 \\ 0.50 & 1.00 \end{pmatrix}, \quad (17)$$

such that,

$$\begin{pmatrix} \mathbf{b}_1 \\ \mathbf{b}_2 \end{pmatrix} = \mathbf{M} \cdot \begin{pmatrix} \mathbf{a}_1 \\ \mathbf{a}_2 \end{pmatrix} = \begin{pmatrix} 11.00 & 0.00 \\ 0.50 & 1.00 \end{pmatrix} \cdot \begin{pmatrix} \mathbf{a}_1 \\ \mathbf{a}_2 \end{pmatrix}. \quad (18)$$

Here,  $\mathbf{b}_1$  and  $\mathbf{b}_2$  are the reconstructed overlayer unit cell basis vectors, whereas  $\mathbf{a}_1$  and  $\mathbf{a}_2$  are the unreconstructed surface unit cell basis vectors. Note that some of the spots do not align well with the reciprocal unit cells annotated on Figure 10. This can be attributed to the LEED pattern being offset from the centre of the fluorescent screen, resulting in the distances on the LEED pattern being slightly distorted from that of the true reciprocal space. To describe the reconstruction using Wood notation, the following equation can be used:

$$b_1 = \sqrt{m_{11}^2 a_1^2 + m_{12}^2 a_2^2 + 2(m_{11}m_{12})(a_1a_2) \cos \gamma} \quad (19)$$

where  $m_{11}$  and  $m_{12}$  are elements of  $\mathbf{M}$ , and  $\gamma$  is the angle of the underlayer surface unit cell. For Au(111),  $a_1 = a_2 = a$  (as demonstrated in Section 3.3), and  $\gamma = 120^\circ$ . This simplifies to,

$$\frac{b_1}{a} = \sqrt{m_{11}^2 + m_{12}^2 - m_{11}m_{12}} \quad (20)$$

The same applies to  $\mathbf{b}_2$ , and its corresponding matrix elements,  $m_{21}$  and  $m_{22}$ .

The Wood notation is defined as  $\left(\frac{b_1}{a} \times \frac{b_2}{a}\right)$ . Therefore, using Equation (20), the reconstruction can be described as a  $(11 \times \frac{\sqrt{3}}{2})$  overlayer. Clearly, the calculated unit cell is half the size of the  $(22 \times \sqrt{3})$  unit cell reported by STM studies.<sup>[4]</sup> While a  $(22 \times \sqrt{3})$  LEED pattern would also fit the reconstruction spots perfectly, it would result in more reconstruction spots between  $(0,0)$  and the first order spots for the unreconstructed underlayer. As it is apparent from Figure 10, no reconstruction spots were observed near the midpoint region between  $(0,0)$  and the first order spots. Thus, the  $(11 \times \frac{\sqrt{3}}{2})$  reciprocal cell was chosen as the best-fit explanation for this LEED pattern, as it involved less reconstruction spots than the  $(22 \times \sqrt{3})$  reciprocal cell in literature.<sup>[4]</sup>

### 3.5 LEED pattern for Blue Phosphorus on Au (111)

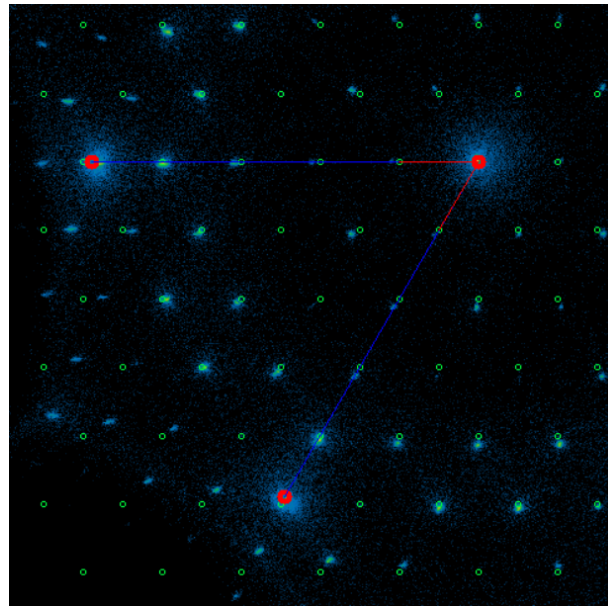


Figure 11: SPA-LEED pattern of P/Au(111). The (111) underlayer spots are labelled red, whereas the phosphorus spots are highlighted green. The reciprocal surface unit cells of the (111) underlayer as well as the reconstructed overlayer are shown, with blue and red reciprocal unit cell basis vectors respectively.

As mentioned, phosphorus was not successfully adsorbed onto Au(111) in this experiment, hence an exemplar SPA-LEED pattern of a P/Au(111) surface was used, carried out at 68 eV. The LEED pattern shown in Figure 11 indicates that phosphorus adsorbs onto Au(111) in a p( $5 \times 5$ ) supercell. This agrees with the value reported by M. Gruenewald *et al.*, in which an LEED of P/Au(111) was recorded at 140.0 eV.<sup>[7]</sup> The overlayer spots do not exactly coincide with the predicted overlayer reciprocal unit cell, as is typical with SPA-LEED experiments.<sup>[8]</sup>

## 4 Discussion

### 4.1 Determination of the LEED-screen to sample distance and the lattice constants

Comparing the solutions for the averaged lattice constants  $a_{\text{total}} = 2.888 \pm 0.088 \text{ \AA}$  and  $a_{b,\text{total}} = 4.084 \pm 0.124 \text{ \AA}$  with the quantities found by B. N. Dutta and B. Dayal.<sup>[6]</sup> shows that the in this experiment measured and calculated data is reasonably good. The difference between calculation and literature lies in a region smaller than  $0.01 \text{ \AA}$ . This leads to the conclusion, that also the calculation for the LEED-screen to sample distance  $r = 627 \pm 16.6$  pixels was successful. One reason for the difference between results and B. N. Dutta and B. Dayal.<sup>[6]</sup> could have been the resolution of the pictures. The program Spot-Plotter only allowed a lower resolution than the one received from the camera. As a result, the resolution was changed to (1260x945) pixels per picture, to have the same resolution in all pictures. This change in resolution leads to an inaccuracy in measuring the spots on the pictures and so their distances. The results show, that this difference is rather negligible, if the data is not only calculated out of one measurement but averaged over more data points. It can be said, that the results would have been even closer to the literature, if the calculations were averaged over even more data.

### 4.2 The Au (111) surface reconstruction

Compared to the well-documented  $(22 \times \sqrt{3})$  value,  $(11 \times \frac{\sqrt{3}}{2})$  makes for a significantly smaller overlayer unit cell – exactly a quarter of the size of the unit cell as described in literature.<sup>[4]</sup> An explanation could be that the second order reconstruction spots are higher in intensity than the first order spots. If the second order spots were to be mistaken for first order spots, the resulting overlayer reciprocal unit cell would be  $(11 \times \frac{\sqrt{3}}{2})$ , as is observed in this LEED experiment (Figure 10). Thus, correcting for this error would yield a  $(22 \times \sqrt{3})$  reciprocal lattice. This inversion in intensity was observed in the Helium Atom Scattering of Au(111) by Harten *et al.* as well, who attributed this phenomenon to the strong Fourier coefficients of the second order spots.<sup>[5]</sup> Harten and colleagues further attributed the strong second order Fourier coefficient to the vertical displacement caused by the surface corrugation as a result of the reconstruction.<sup>[5]</sup> This surface corrugation, in turn, is caused by the vertical displacement of the overlayer gold atoms occupying a 2-coordinated “valley” site as opposed to 3-coordinated *hcp* and *fcc* “hollow” sites. STM images from various studies of the Au(111) surface confirm the presence of the surface corrugations.<sup>[4][9]</sup>

### 4.3 The P/Au(111) system

Despite carrying out the procedure of dosing Au(111) with phosphorus, no phosphorus was present on the surface, as the spots corresponding to the phosphorus overlayer was not observed. This was attributed to a malfunction in the phosphorus gun attached to the LEED apparatus. Otherwise, the successful adsorption of phosphorus on Au(111) would give a p( $5 \times 5$ ) overlayer, as demonstrated in Figure 11.

Without any Au-P interactions, a single layer of blue phosphorus honeycomb forms a p( $\sqrt{19} \times \sqrt{19}$ ) supercell on Au(111), which is clearly incommensurate.<sup>[3]</sup> Because of Au-P interactions, as well as lattice mismatch, blue phosphorus reconstructs into a commensurate p( $5 \times 5$ ) buckled honeycomb structure.<sup>[3]</sup> The driving force behind this reconstruction arises from substrate-adsorbate interactions dominating adsorbate-adsorbate interactions in the same monolayer.<sup>[2]</sup> In the case for P/Au(111), it is energetically more favourable to strain certain P-P covalent bonds for stronger Au-P chemisorptive interactions than to maintain the unstrained honeycomb structure of a blue phosphorus monolayer.<sup>[3]</sup> Since a p( $5 \times 5$ ) LEED pattern was observed instead of p( $\sqrt{19} \times \sqrt{19}$ ), this confirms the presence of strong Au-P interactions resulting in blue phosphorus adopting the buckled honeycomb structure. This is further supported by STM images of P/Au(111) showing the same p( $5 \times 5$ ) supercell.<sup>[7]</sup> These findings also imply that Au(111) may not be the best surface for the synthesis of blue phosphorus.

It can also be noted that the reconstruction spots corresponding to the ( $22 \times \sqrt{3}$ ) Herringbone reconstruction were not observed in the SPA-LEED pattern of P/Au(111). However, this is not enough evidence to conclusively prove that the Herringbone reconstruction is not present in the blue phosphorus overlayer. Perylenetetracarboxylic dianhydride (PTCDA) adsorption experiments for blue phosphorus on Au(111) indicate that the PTCDA overlayer follows a Herringbone pattern.<sup>[7]</sup> This suggests that the morphology of the Herringbone reconstruction must have been transferred onto the blue phosphorus overlayer, which would account for PTCDA forming a Herringbone overlayer. It is therefore apparent that LEED alone does not provide enough information in elucidating the morphology of a surface. To further characterise a surface, one must use imaging techniques such as STM, Atomic Force Microscopy (AFM), or spectroscopic techniques such as Ultraviolet Photoelectron Spectroscopy (UPS) or Temperature Programmed Desorption (TPD).

## References

- [1] M. P. Seah, W. Dench, *Surface and Interface Analysis* **1979**, *1*, 2–11.
- [2] G. Attard, C. Barnes, *Surfaces*, Oxford Science Publications, **1998**.
- [3] S. Zhao, J. L. Zhang, W. Chen, Z. Li, *The Journal of Physical Chemistry C* **2019**, *124*, 2024–2029.
- [4] P. Li, F. Ding, *Science advances* **2022**, *8*, eabq2900.
- [5] U. Harten, A. Lahee, J. P. Toennies, C. Wöll, *Physical review letters* **1985**, *54*, 2619.
- [6] B. N. Dutta, B. Dayal, *physica status solidi (b)* **1963**, *3*, 473–477.
- [7] M. Gruenewald, M. Schaal, I. Karadzhov, L. Brill, J. Domke, P. Grimm, F. Otto, J. Picker, P. M. Simon, H. Tamm, et al., *Physical Review Materials* **2022**, *6*, 015601.
- [8] F. Sojka, M. Meissner, C. Zwick, R. Forker, T. Fritz, *Review of Scientific Instruments* **2013**, *84*.
- [9] R. Staub, M. Toerker, T. Fritz, T. Schmitz-Hübsch, F. Sellam, K. Leo, *Langmuir* **1998**, *14*, 6693–6698.